High-Speed Interrogation of Multiplexed Fiber Bragg Gratings With Spectral Distortion

Bram Van Hoe, Kyle G. Oman, Geert Van Steenberge, Nikola Stan, Stephen M. Schultz, and Kara J. Peters

***Abstract*— Fiber Bragg grating (FBG) sensors can be multiplexed in large numbers to monitor the performance of large structures. This paper addresses the collection of FBG reflection spectra from wavelength division multiplexed sensors at fast acquisition rates. The spectral and temporal resolution is first derived as a function of the tunable filter and measurement system properties. The method is applied to impact loading investigations of a stiffened composite skin panel. The reflected spectrum of each FBG in an array, embedded in the panel, is collected at 100 kHz during the impact events with a spectral resolution down to 40 pm. Visualization of the FBG responses to these impact events, including the presence of spectral distortion in some FBG spectra, is presented. Future analyses based on the full-spectral data sets can enable the assessment of the localized progression of internal damage in such structures.**

***Index Terms*— Bragg gratings, delamination, nondestructive testing, tunable filters, sensor systems.**

I. Introduction

FIBER Bragg Grating (FBG) sensor arrays are increasingly used for dynamic measurements in structural applications. One key to their success is the fact that many FBGs can be multiplexed along a single, lightweight optical fiber, therefore large regions of a structure can be monitored simultaneously. Acquiring data from multiple sensors can be challenging, however, particularly at fast acquisition rates.

Numerous methods of interrogating multiplexed FBGs have been applied, including those based on scanning tunable filters, diffraction gratings, Arrayed Waveguide Gratings (AWGs), and matched edge filters [1]–[6]. John *et al.* [1] provide an excellent review of instrumentation for dynamic strain measurements using FBG sensor arrays. The performance of different interrogation methods depends on the information to be collected. Some data acquisition techniques (like matched filter arrays) provide the wavelength shift of each FBG while some, like scanning tunable filters or expansion of the output beam onto a diffraction grating can resolve the complete reflected spectrum of each FBG.

Edge filters can provide extremely high data acquisition rates, however they require a matched filter for every sensor and are sensitive to intensity variations of the laser source. As an alternative, AWGs can also provide wavelength shifts at fast acquisition rates, furthermore they are not sensitive to source intensity variations since a ratio of matched filters are used. However, both of these techniques do not provide a measurement of the individual FBG reflection spectra and are therefore sensitive to changes in the FBG sensor spectral edge slope. Spectral distortion can be present due to partial disbonding of a surface mounted sensor, transverse loading on an embedded sensor or non-uniform strain along the FBG axis, for example when a wave propagates through the structure [7]. As the edge filter and AWG output rely on a constant reflected spectrum, distortion to the FBG spectra creates apparent wavelength shifts.

In this work, we address the task of collecting the full transient spectral information from a series of multiplexed FBG sensors. This information can either be used to correct for the spectral distortion described above [8], or to provide additional information on the strain distribution near the sensor [9]. Of the techniques to collect optical spectra, scanning tunable filters provide better wavelength resolution than others, however the requirement for a moving component limits the filter driving speed. Due to their low mass, Microelectromechanical System (MEMS) filters can be driven at suitable frequencies for dynamic structural measurements.

The authors previously demonstrated the measurement of the reflected spectrum of a single FBG sensor at acquisition rates up to 300 kHz using a MEMS tunable filter [8]. In this paper we perform dynamic measurements of multiplexed FBG sensors, collecting full-spectral information, up to 100 kHz, with a 21 pm spectral resolution. We also develop design guidelines for the tradeoff between acquisition rate, temporal resolution, spectral resolution, and number of FBGs to be addressed. The measurement technique is demonstrated for an FBG array embedded in a stiffened carbon-fiber epoxy panel for measurements during low-velocity impacts.

II. Interrogation System

The FBG reflected spectra were collected with a dynamic interrogator recently developed by the authors.

Manuscript received July 21, 2017; revised August 28, 2017; accepted August 30, 2017. Date of publication September 8, 2017; date of current version October 11, 2017. This work was supported by the Erasmus Mundus Program of the European Commission under the Transatlantic Partnership for Excellence in Engineering–TEE Project. This paper was presented at the IEEE Sensors 2014 Conference, Valencia, Spain, November 3, 2014. The associate editor coordinating the review of this paper and approving it for publication was Dr. Minghong Yang. *(Corresponding author: Kara J. Peters.)*

B. Van Hoe is with the Department of Mechanical and Aerospace Engineering, North Carolina State University, Raleigh, NC 27695 USA, and also with the Centre for Microsystems Technology, Elis Department, Ghent University–IMEC, B-9052 Ghent, Belgium (e-mail: bramvanhoe@gmail.com)

K. G. Oman and K. J. Peters are with the Department of Mechanical and Aerospace Engineering, North Carolina State University, Raleigh, NC 27695 USA (e-mail: kjpeters@ncsu.edu).

G. Van Steenberge is with the Centre for Microsystems Technology, Elis Department, Ghent University–IMEC, B-9052 Ghent, Belgium.

N. Stan and S. M. Schultz are with the Department of Electrical and Computer Engineering, Brigham Young University, Provo, UT 84602 USA (e-mail: schultz@ee.byu.edu).

Digital Object Identifier 10.1109/JSEN.2017.2750327

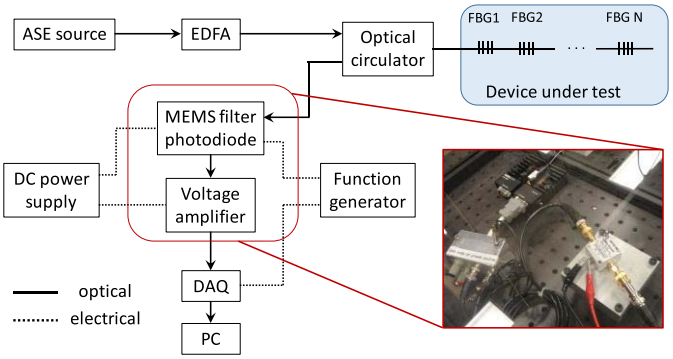

Fig. 1. Schematic view of the interrogation system.

Complete details of the interrogator and post-processing of the data are found in Vella et al. [2]. The FBG spectra interrogation scheme is based on a broadband optical source and a MEMS tunable filter allowing for wavelength demodulation, as shown in Fig. 1. An Erbium Doped Fiber Amplifier (EDFA) is used to amplify the output spectrum of the Amplified Stimulated Emission (ASE) source. The reflected output of the FBG sensor array passes through the MEMS tunable Fabry Perot filter, pre-packaged with a photodiode. The DC power supply and function generator drive the electrostatic membrane in the tunable filter with the DC voltage determining the center wavelength and the AC voltage driving the filter with a sinusoidal input determining the wavelength range and interrogation frequency. Driving the filter with a sinusoidal voltage creates a steady state Fabry Perot interference condition, eliminating filter overshoot problems. The MEMS filter can be driven at a maximum frequency of 300 kHz. Real-time data storage and post-processing overcomes the need for real-time processing. The output of the MEMS filter is amplified with a transimpedance amplifier and acquired with a high-speed Data Acquisition (DAQ) card. In order to calibrate the wavelength to time conversion, the ASE source and FBG sensor were replaced with a tunable laser, scanned at known wavelengths, as described in [2]. A second-order Chebyshev stop-band filter was applied to each data set prior to processing the time-varying data to eliminate periodic noise that appeared in the measured optical power. In this paper, the filter sweep rate was limited to 100 kHz, as the spectral resolution decreases above 125 kHz with the particular DAQ card.

The authors previously demonstrated the acquisition of the reflection spectrum of a single FBG at acquisition rates up to 300 kHz [8]. For such measurements, the minimum wavelength range can be collected to maximize the wavelength resolution. However, when considering the measurement of FBG sensor arrays during dynamic events, two important parameters of the interrogation system must be tuned, the average wavelength resolution $\Delta\lambda_{\text{ave}}$ and the temporal resolution, Δt. There is a tradeoff between these resolution numbers and the bandwidth required for the interrogator (i.e. the number of sensors to be multiplexed). Depending on the needs of the application, the wavelength window, W, the average wavelength resolution, $\Delta\lambda_{\text{ave}}$, temporal resolution Δt, total measurement time, T_{meas}, or the spectral scanning

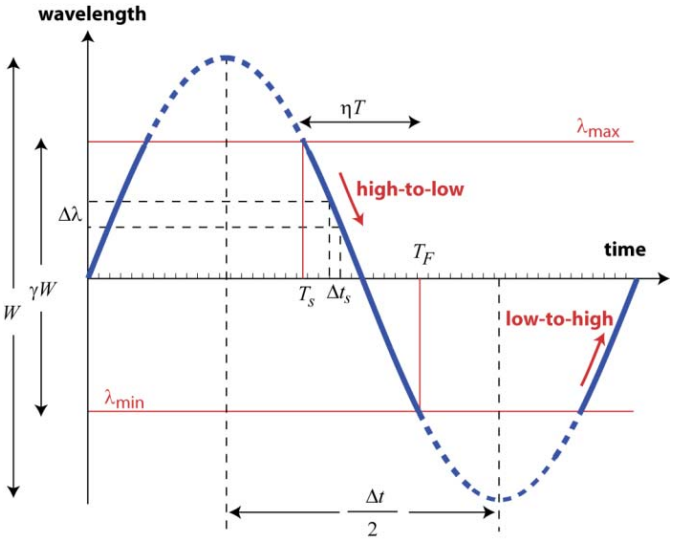

Fig. 2. Schematic of filter wavelength output for one sweep. Solid blue line is measurement range, dashed blue line is outside of measurement range.

rate (defined as the filter driving frequency), f_{MEMS}, can be maximized. The temporal resolution is inversely proportional to the MEMS filter driving frequency,

$$\Delta t = \frac{1}{f_{MEMS}} \tag{1}$$

If M is the maximum number of data points that can be collected due to hardware restrictions, determined by the maximum data file size, then T_{meas} is defined as,

$$T_{meas} = \frac{M}{f_s} \tag{2}$$

where f_s is the data acquisition card sampling rate. For our system, $M = 3.33 \times 10^7$ and 10 MHz $\leq f_s \leq$ 100 MHz.

Calculating the total number of samples collected in a given sweep, $W/\Delta\lambda_{\text{ave}}$, times the total number of filter sweeps, T_{meas}/Δt, we find the upper limit relationship between the average wavelength resolution and temporal resolution,

$$\frac{W T_{meas}}{\Delta t \, \Delta\lambda_{ave}} \leq M \tag{3}$$

Fig. 2 shows the filter wavelength output for one sweep. The sections of the wavelength sweep where the wavelength sensitivity is very low are removed from the data sets during post-processing of the data. These are shown as the dashed line in Fig. 2. The time fraction of the data used is labelled as η. Both the high-to-low or low-to-high wavelength sweeps of the data are set can be used.

It is important to note that in (3), $\Delta\lambda_{\text{ave}}$ is the average wavelength resolution, since the wavelength resolution varies throughout a given sweep, while the time resolution is constant. The filter output wavelength as a function of time is given as

$$\lambda = \frac{W}{2} \sin\left(2\pi f_{MEMS} t\right) \tag{4}$$

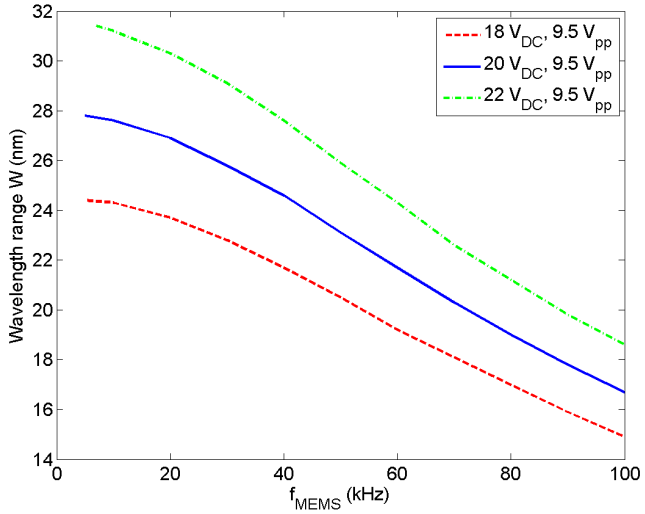

Fig. 3. Wavelength window as a function of the driving voltage and driving frequency of the MEMS tunable filter.

and the wavelength resolution as a function of time can be determined as,

$$\Delta\lambda = W\pi f_{MEMS}\,\Delta t_s \cos\left(2\pi f_{MEMS} t\right) \tag{5}$$

where $\Delta t_s = 1/f_s$ is the sampling time step.

As shown in Fig. 2, the measurement starting time $T_S = (\Delta t/2)(1-\eta/2)$ and finishing time, $T_F = (\Delta t/2)(1+\eta/2)$. Using $\eta = 0.4$ (as in our experiments), the mean value $\Delta\lambda_{\text{ave}} = 0.940\ (W\pi f_{\text{MEMS}}\Delta t_s)$, while the maximum and minimum wavelength resolutions are $\Delta\lambda_{\text{min}} = 0.87\ \Delta\lambda_{\text{ave}}$ and $\Delta\lambda_{\text{max}} = 1.07\ \Delta\lambda_{\text{ave}}$. In addition, the measurement window range is also narrowed to $W_f = \gamma W$, with $\gamma = \sin[\pi(1-\eta/2)]$, in this case 0.59. Eq. (3) should therefore be written,

$$\frac{W_f T_{meas}}{\gamma\,\Delta t\,\Delta\lambda_{ave}} \le M \tag{6}$$

in terms of the final measurement wavelength window, W_f.

Finally, the wavelength window W is inherently related to the MEMS filter driving frequency through the mechanical vibration of the electrostatically activated membrane. This dependency is linked to both the DC applied voltage (defining the central wavelength) and the superimposed AC driving voltage (defining the wavelength sweeps). Fig. 3 depicts the measured wavelength range as a function of the filter driving frequency using different DC voltage inputs. 9.5 Vpp is the maximum sweeping voltage used in these experiments.

Fig. 4 plots the mean wavelength resolution vs. time resolution obtained using (3) and the 20 V_{DC} filter data of Fig. 3 for different filter driving frequencies and measurement times. For these calculations, the maximum sampling rate $f_s = 100$ MHz was applied. The maximum and minimum measurement times for this configuration are 3.333 and 0.333 seconds respectively. To determine the absolute measurement accuracy of the interrogation system for a given FBG reflection spectrum, one would also have to consider the spectral bandwidth of the MEMS tunable filter which is around 60 pm.

As a proof-of-principle experiment, an FBG chain (multiplexed in a single optical fiber, spectral spacing of 2 nm)

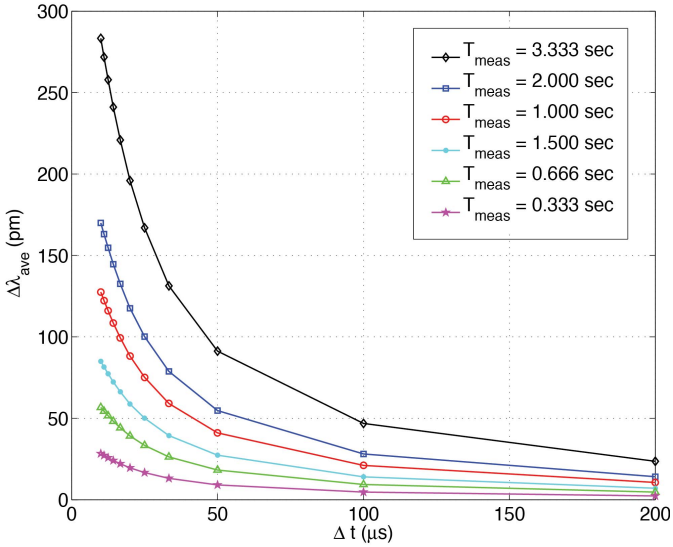

Fig. 4. Mean wavelength resolution as a function of filter driving frequency for $f_s = 100$ MHz and filter driving voltage of 20 V_{DC}, 9.5 V_{pp}.

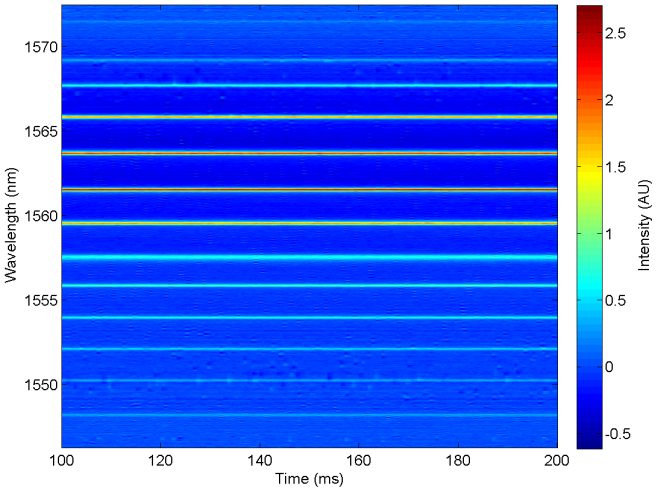

Fig. 5. Full-spectral reconstruction of 13 FBG sensors using a filter driving voltage of 20 V_{DC} and 9 V_{pp} at $f_{\text{MEMS}} = 10$ kHz. The resulting interrogation system characteristics are $\Delta t = 0.1$ ms and $\Delta\lambda_{\text{ave}} = 3$ pm using a data acquisition frequency $f_{\text{DAQ}} = 100$ MHz.

was addressed using different acquisition parameters. Full-spectral datasets are visualized through color plots showing the relative reflected optical power. An example is shown in Fig. 5. Setting the voltage modulation signal to 9 V_{pp} at 10 kHz, 13 sensors can be read out simultaneously without compromising the performance in terms of spectral resolution [10]. The varying grating reflectivity in Fig. 5 is due to the non-uniform output spectrum of the EDFA. This effect can be compensated for in the data post-processing as will be shown in the results of the impact loading tests.

III. Impact Loading on Integrally Stiffened Panel With Embedded FBG Sensor Array

The high-speed interrogation system was characterized for a FBG sensor array embedded in an integrally stiffened carbon-fiber composite panel subjected to low-velocity impacts.

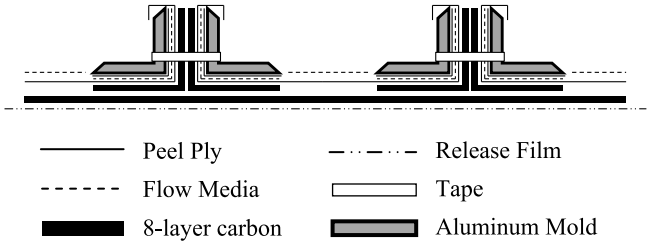

Fig. 6. Schematic build-up (layup cross section) of integrally stiffened specimen.

Fabricating stiffeners and the skin panel in a single process produces a relatively strong aerospace component, without the need to bond the stiffeners to the skin. However such components still present challenges for durability, as critical impact induced damage cannot necessarily be observed on the panel surface. Therefore FBG sensors integrated in the component can provide additional information on the severity of impact events and the resulting damage to the structure.

The two T-shaped stringers were integrally cured with the skin panel using Vacuum Assisted Resin Transfer Molding (VARTM). The sensor array was directly embedded at the midplane of the skin during layup of the panel. The dry carbon fabric was layed up on a waxed metal mold, with layers of peel ply and flow media to produce a uniform resin flow across the part, as shown in Fig. 6. Details of the fabrication process can be found in [11]. The skin and stiffener stacking sequences were $(+45°/-45°/0°/90°)_S$.

The FBG sensors are Draw Tower Gratings® from FBGS International [12], multiplexed with a 2 cm spacing in a single optical fiber, with peak wavelengths between 1530 and 1590 nm. Fig. 7 shows the location of the embedded optical fibers, FBG sensors and the impact locations. The optical fiber was placed in the middle of the 8-layer carbon layup of the base panel prior to layup of the stiffeners. The optical fiber inlet and outlets were sandwiched between release film layers to prevent adhesion to the vacuum bag. Figure 8 shows the final VARTM layup after vacuum bagging including the panel, optical fibers and vacuum bag. Once a vacuum was drawn, the entire assembly cured at room temperature for 24 hours.

An example of a final specimen after resin infusion, curing and removal of the mold is shown in Fig. 9. Impact loading experiments were performed manually using an impact hammer at the locations shown in Fig. 7. The specimen was clamped on the long edges and the panel was impacted on the surface opposite to the stiffeners (skin side).

IV. Measurement Results

The embedded sensor responses were acquired during 6 impact events. Fig. 10 (impact 3) and Fig. 11 (impact 4) show examples of these measurements during 2 consecutive impacts. All impact measurements are referenced to the EDFA output spectrum to compensate for the non-uniform optical intensity. These were the first two impacts relatively close to the middle FBG sensors shown in Fig. 7 (λ_B = 1558 to 1566 nm). The dynamic impact waves are clearly visible

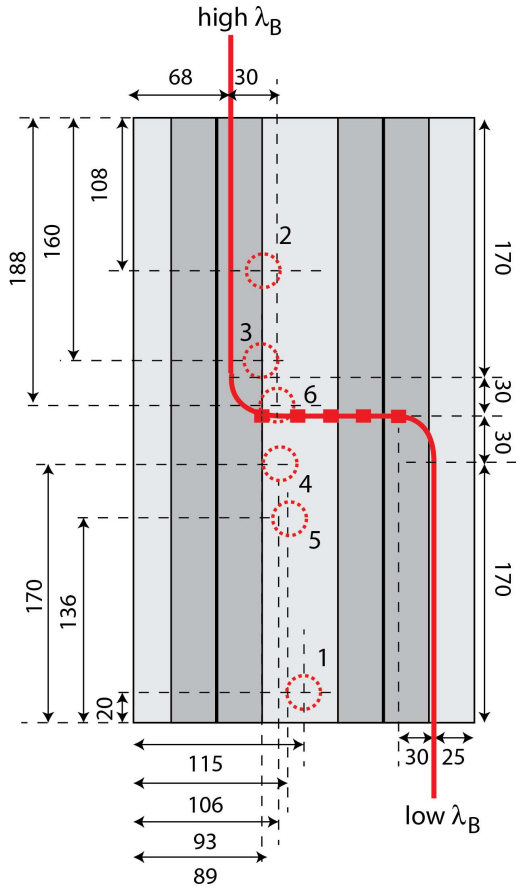

Fig. 7. Location of embedded FBG sensors and optical fiber in integrally stiffened panel. All dimensions in mm. Location of 5 FBGs in horizontal section are shown (λ_B = 1558 to 1566 nm). Impact locations (applied on skin surface) shown as circles.

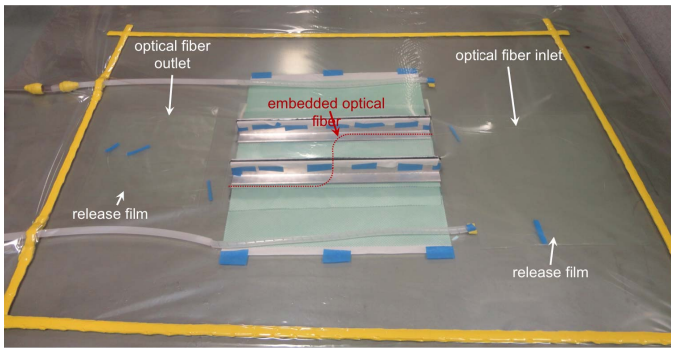

Fig. 8. VARTM vacuum bag including resin inlet and outlet, optical sensing fiber, aluminum stiffener molds, carbon fiber layup, peel ply and flow media.

in the different graphs. Figs. 10 and 11 are measured using a temporal resolution of 0.1 ms. Several discontinuities are visible Fig. 11, for example at t = 371 ms. These discontinuities indicate a need for an increased temporal resolution. The resolution was therefore changed to 0.01 ms during the next impact events. Fig. 12 shows the response acquired during impact 6. This impact was extremely close to the sensors with λ_B = 1566 and 1564 nm. Because of the increased filter driving frequency, the wavelength window was reduced, limiting the number of addressable sensors.

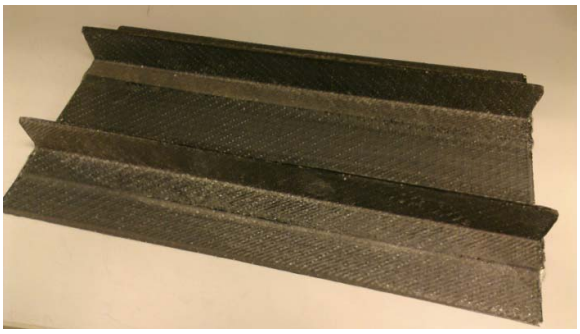

Fig. 9. Integrally stiffened composite panel after releasing it from the vacuum set-up.

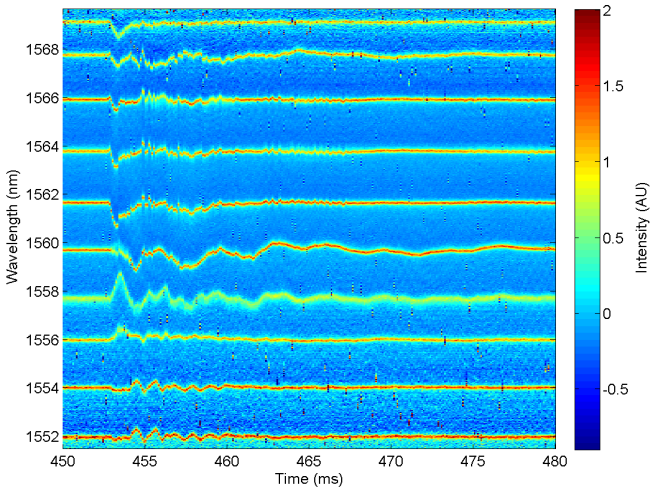

Fig. 10. Full-spectral reconstruction of 10 FBG sensors during an impact event (impact 3) using a filter driving voltage of 20 V_{DC} and 6 V_{pp} at 10 kHz. The resulting interrogation system characteristics are $\Delta t = 0.1$ ms and $\Delta\lambda = 4$ pm using a data acquistion frequency $f_S = 50$ MHz.

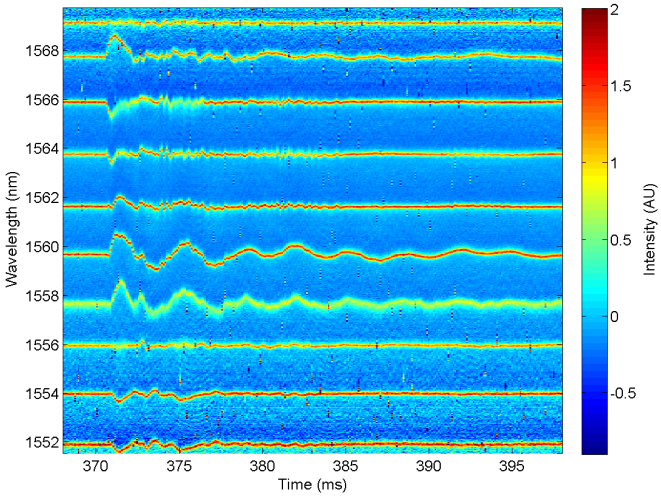

Fig. 11. Full-spectral reconstruction of 10 FBG sensors during an impact event (impact 4) using a filter driving voltage of 20 V_{DC} and 6 V_{pp} at 10 kHz. The resulting interrogation system characteristics are $\Delta t = 0.1$ ms and $\Delta\lambda = 4$ pm using a data acquistion frequency $f_S = 50$ MHz.

These full-spectral measurements enabled the detection of non-uniform and asymmetric loading events involving peak broadening and/or splitting. Fig. 13 shows a detailed view of Fig. 12 (impact 6) on one FBG sensor with $\lambda_B = 1566$ nm,

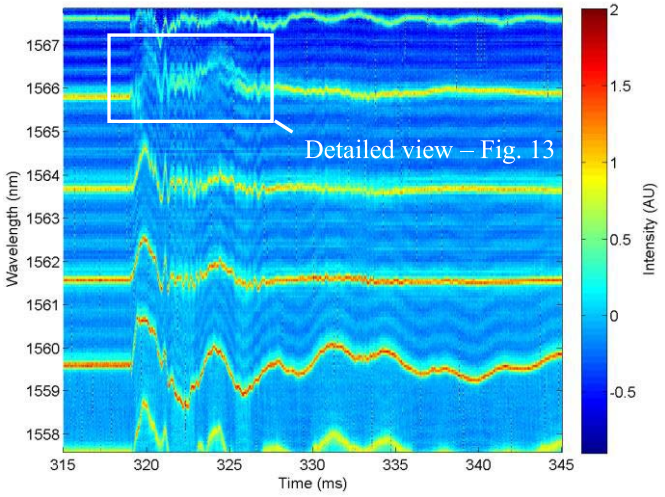

Fig. 12. Full-spectral reconstruction of 6 FBG sensors during an impact event (impact 6) using a filter driving voltage of 19.4 V_{DC} and 6 V_{pp} at 100 kHz. The resulting interrogation system characteristics are $\Delta t = 0.01$ ms and $\Delta\lambda = 21$ pm using a data acquistion frequency $f_S = 50$ MHz.

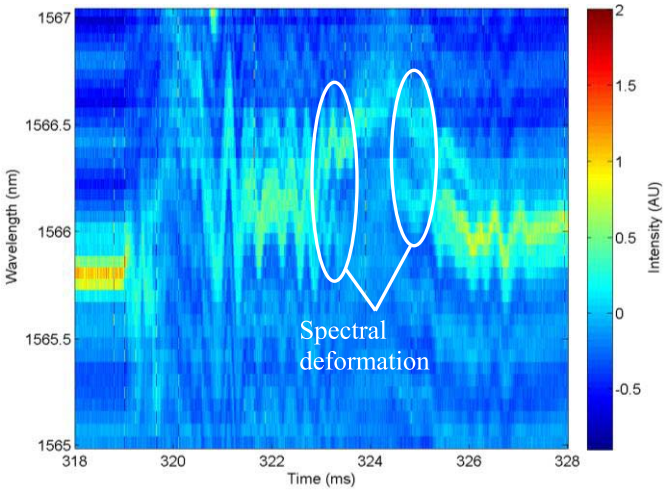

Fig. 13. Detailed view on 1 FBG sensor during an impact event (Fig. 12 – impact 6).

which showed considerable spectral distortion during the impact. Due to the spectral distortion, it would be difficult to determine the induced strain history at this sensor during the impact.

Selected spectral sweeps from impact 4 are plotted in Fig. 14. Fig. 14(a) highlights one sensor whose signal remained a uniform peak throughout the impact, while the reflected peak of the sensor shown in Fig. 14(b) was damped out at around 374 ms. Fig. 14(c) shows the displacement of the spectrum of one of the sensors with successive measurement sweeps of the interrogator.

Similar selected spectral sweeps are plotted from impact 6 in Fig. 15. The time resolution is 10 times higher for these measurements, so we observe that the temporal resolution is sufficient to capture the spectral shifts in Fig. 15(c), however we can also see the reduced wavelength resolution through the fact that the Gaussian shape of the reflected peaks are poorly

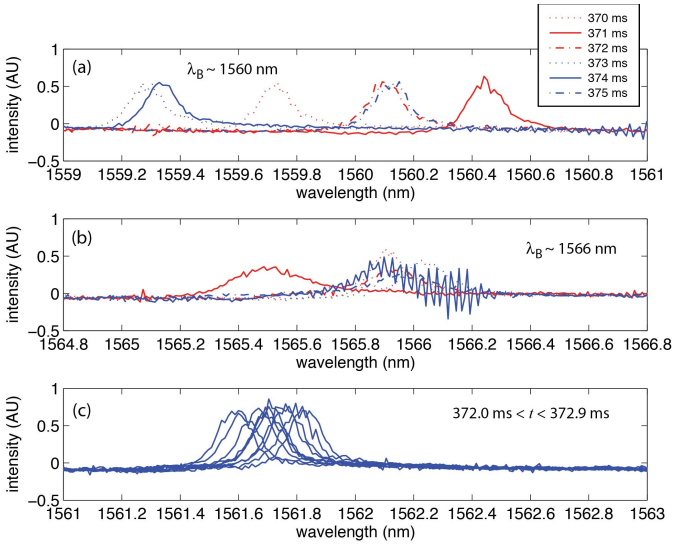

Fig. 14. Individual spectral sweeps collected during impact 4: selected mesaurements of FBG sensors with $\lambda_B\sim$ (a) 1560 nm and (b) 1566 nm, collected at 1 ms intervals; (c) ten successive measurements of FBG sensor with $\lambda_B \sim 1562$ nm. Full measurements can be seen in Fig. 11.

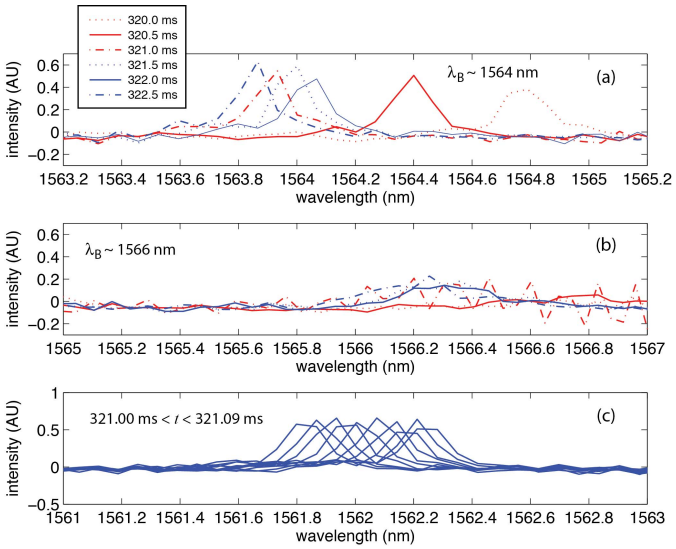

Fig. 15. Individual spectral sweeps collected during impact 6: selected mesaurements of FBG sensors with $\lambda_B\sim$ (a) 1564 nm and (b) 1566 nm, collected at 0.5 ms intervals; (c) ten successive measurements of FBG sensor with $\lambda_B \sim 1562$ nm. Full measurements can be seen in Fig. 12.

reconstructed. Fig. 15(b) shows an example of one of the sensors that was near the impact (the same sensor of Fig. 13) and whose reflected spectrum was lost temporarily during the impact (near 321 ms). It is not expected that better wavelength resolution would improve the strain measurement, but that the physical conditions for strong reflectivity was temporarily lost in the FBG. This effect is stronger than that seen in Fig. 14(b), due to the close proximity of the sensor to the impact location.

V. Conclusions

To fully exploit the advantages of FBGs, there is a need for high-speed, dynamic read-out measurements capturing the full spectral information of a series of multiplexed sensors. Within this paper, an interrogation system based on a tunable MEMS photodiode was evaluated to interrogate up to 13 FBG sensors in a single measurement. This system is capable of reading out FBG spectral datasets up to 100 kHz. The accuracy both in terms of spectral and temporal resolution are linked through the dynamic characteristics of the interrogation set-up. Depending on the needs of the application (high-speed, small perturbations, …), the interrogation system enables a spectral resolution down to a few pm and a temporal resolution down to 10 μs. Detailed visualization of impact loading experiments on integrally stiffened composite panels were presented to show the high-speed and full-spectral capabilities of the interrogation system.

References

[1] R. N. John, I. Read, and W. N. MacPherson, "Design considerations for a fibre Bragg grating interrogation system utilizing an arrayed waveguide grating for dynamic strain measurement," *Meas. Sci. Technol.*, vol. 24, no. 7, p. 075203, Jul. 2013.

[2] T. Vella *et al.*, "Full-spectrum interrogation of fiber Bragg gratings at 100 kHz for detection of impact loading," *Meas. Sci. Technol.*, vol. 21, no. 9, p. 094009, Sep. 2010.

[3] G. Xiao, N. Mrad, F. Wu, Z. Zhang, and F. Sun, "Miniaturized optical fiber sensor interrogation system employing echelle diffractive gratings demultiplexer for potential aerospace applications," *IEEE Sensors J.*, vol. 8, no. 7, pp. 1202–1207, Jul. 2008.

[4] Y. S. Kwon *et al.*, "Dynamic sensor interrogation using wavelength-swept laser with a polygon-scanner-based wavelength filter," *Sensors*, vol. 13, no. 8, pp. 9669–9678, Jul. 2013.

[5] L. Yan, Z. Wu, Z. Zhang, W. Pan, B. Luo, and P. Wang, "High-speed FBG-based fiber sensor networks for semidistributed strain measurements," *IEEE Photon. J.*, vol. 5, no. 2, Apr. 2013, Art. no. 7200507.

[6] Y. Sano and T. Yoshino, "Fast optical wavelength interrogator employing arrayed waveguide grating for distributed fiber Bragg grating sensors," *J. Lightw. Technol.*, vol. 21, no. 1, pp. 132–139, Jan. 2003.

[7] S. Yashiro and T. Okabe, "Estimation of fatigue damage in holed composite laminates using an embedded FBG sensor," *Compos. A, Appl. Sci. Manuf.*, vol. 42, no. 12, pp. 1962–1969, Dec. 2011.

[8] S. Webb *et al.*, "Wavelength hopping due to spectral distortion in dynamic fiber Bragg grating sensor measurements," *Meas. Sci. Technol.*, vol. 22, no. 6, p. 065301, Jun. 2011.

[9] A. Propst *et al.*, "Assessment of damage in composite laminates through dynamic, full-spectral interrogation of fiber Bragg grating sensors," *Smart Mater. Struct.*, vol. 19, no. 1, p. 015016, Jan. 2010.

[10] B. van Hoe, K. Oman, K. Peters, N. Stan, and S. Schultz, "High-speed interrogation of multiplexed fiber Bragg gratings enabling real-time visualization of dynamic events such as impact loading," in *Proc. IEEE Sensors Conf.*, Nov. 2015, pp. 402–405.

[11] K. Oman *et al.*, "Instrumentation of integrally stiffened composite panel with fiber Bragg grating sensors for vibration measurements," *Smart Mater. Struct.*, vol. 24, no. 8, p. 085031, Jul. 2015.

[12] FBGS. *Draw Tower Gratings (DTGS)*. Accessed: Aug. 27, 2017. [Online]. Available: http://www.fbgs.com/

Bram Van Hoe received the M.Sc. and Ph.D. degrees in electrical engineering from Ghent University, Belgium, in 2008 and 2013, respectively. He joined the Centre for Microsystems Technology, an IMEC Associated Research Laboratory at Ghent University. He was a Post-Doctoral Researcher and spent six months with the Department of Mechanical and Aerospace Engineering, North Carolina State University within the framework of the Transatlantic Partnership for Excellence in Engineering. He is currently a Business and Technology Developer with FBGS International.

Kyle G. Oman received the B.S. degree in mechanical engineering in 2012 and the M.S. degree in aerospace engineering in 2014 from North Carolina State University. He is currently a Structural Analysis Engineer, The Boeing Company.

Geert Van Steenberge received the degree in electrical engineering and the Ph.D. degre in engineering sciences from Ghent University, Belgium in 2002 and 2006. Since 2006, he has been with the Centre for Microsystems Technology, IMEC Associated Laboratory, Ghent University, where he is currently the Head with the Polymer Photonics and Laser Technology Research Team. Since 2012, he has been a part-time Professor with the Electronics and Information Systems Department. Under his supervision, the group has built up a technology and photonic packaging platform allowing for the integration of optical waveguides, coupling structures, light sources, detectors, and electronic circuitry with both rigid, flexible, and stretchable substrates.

Nikola Stan was born in Baden, Switzerland, in 1978 and raised in Belgrade, Serbia. He received the B.S. degree in electrical engineering from the School of Electrical Engineering, University of Belgrade, Serbia, in 2010. He is currently pursuing the Ph.D. degree in electrical engineering with Brigham Young University, Provo, UT, USA. He is currently a Research Assistant with Brigham Young University.

Stephen M. Schultz received B.S. and M.S. degrees in electrical engineering from Brigham Young University, Provo, UT, USA, in 1992 and 1994, respectively, and the Ph.D. degree in electrical engineering from the Georgia Institute of Technology, Atlanta, GA, USA, in 1999. He was with Raytheon Missile Systems from 1999 to 2001. In 2002, he joined the Faculty of the Department of Electrical and Computer Engineering, Brigham Young University, where he conducts research on optical fiber devices.

Kara J. Peters received the Ph.D. degree in aerospace engineering from the University of Michigan in 1996. Until 2000, she was a Research Collaborator with the Laboratory of Applied Mechanics and Reliability, Ecole Polytechnique Fédérale de Lausanne, Switzerland. In 2000, she joined the Faculty of the Department of Mechanical and Aerospace Engineering at North Carolina State University, where she conducts research on optical fiber sensors and their application to experimental mechanics.